ACS APPLIED MATERIALS & INTERFACES

Research Article

www.acsami.org

Mesochanneled Hierarchically Porous Aluminosiloxane Aerogel Microspheres as a Stable Support for pH-Responsive Controlled Drug Release

Linsha Vazhayal,[†] Sindhoor Talasila,[‡] Peer Mohamed Abdul Azeez,[†] and Ananthakumar Solaiappan*[,†]

[†]Functional Materials Section, Materials Science and Technology Division, Council of Scientific and Industrial Research, National Institute for Interdisciplinary Science and Technology (CSIR-NIIST) Thiruvananthapuram, 695019 Kerala, India

[‡]Department of Pharmaceutics, K. M. College of Pharmacy, Uthangudi, Melur Road, Madurai, 625107 Tamilnadu India

Supporting Information

ABSTRACT: The molecular-scale self-assembly of a 3D aluminosiloxane (Al−O−Si) hybrid gel network was successfully performed via the cocondensation of hydrolyzed alumina (AlOOH) and (3-aminopropyl)trimethoxysilane (APS). It was transformed into a microspherical aerogel framework of Al−O−Si containing mesochannels with tunable hierarchically bimodal meso/macroporosities by a subcritical drying technique. Good homogeneity of AlOOH and APS brought during the synthesis guaranteed a uniform distribution of two metal oxides in a single body. A systematic characterization of the aerogel support was carried out using FTIR, SEM, TEM, nitrogen adsorption/desorption analysis, WAXS, SAXS, and ξ-potential measurement in order to explore the material for drug uptake and release. The drug loading and release capacity and chemical stability of an aluminosiloxane aerogel were studied using two nonsteroidal antiinflammatory drugs, ibuprofen and aspirin. A comprehensive evaluation of the aluminosiloxane aerogel with ordered mesoporous MCM-41 was also performed. Aerogel supports showed a high drug loading capacity and a pH-responsive controlled-release property compared to MCM-41. Meanwhile, kinetic modeling studies indicate that the drug releases with a zero-order profile following the Korsmeyer−Peppas model. The biocompatibility of aluminosiloxane aerogels was established via ex vivo and in vivo studies. We also outline the use of aluminosiloxane aerogel as a support for a possible 3D matrix for an osteoconductive structure for bone tissue engineering.

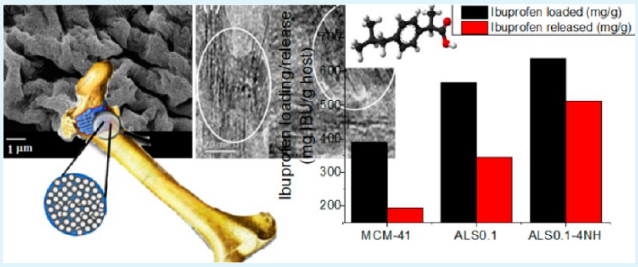

KEYWORDS: *sol−gel synthesis, aerogel microspheres, hierarchically structured bimodal porosities, controlled drug-delivery system, biocompatibility, pH-responsive*

1. INTRODUCTION

Drug-delivery research in biomaterial science was centered toward the design and development of effective molecular supports for drug loading and its delivery specifically to the targeted location at a controlled release rate. Designing a controlled drug-delivery system (DDS) requires the simultaneous consideration of several factors such as the retention of a drug property, route of administration, nature of the delivery vehicle, mechanism of drug release, ability of targeting, and biocompatibility.[1,2] To date, polymeric species including biopolymers and hydrogels have been found to be successful for DDSs and widely reported in the literature. However, in such polymer-based carriers, the use of cross-linking functional groups is necessary to chemically attach the drug molecules.[3−5] The advancement in materials science is now showing inorganic porous materials as very promising candidates for numerous drug-delivery applications.[1] Inorganic porous materials satisfy most of the critical properties, such as high surface area, tunable porosity, uniform pore-size distribution, and stable pore structures with defined surface characteristics, that are needed for the effective loading of drugs.[1,6−8] Ordered mesoporous materials like MCM-41, MCM-48, SBA-15, hexagonal mesoporous silica, and TUD-1 with foamlike mesoporous structure have emerged as promising drug carriers in the category of inorganic supports, and they are well explored as DDSs in recent years.[2,7−15] In such siliceous porous systems, the pore geometry is mostly monomodel; single-type molecular pores ranging from 2 to 50 nm limit the loading of multiple drugs and large-size drug molecules. Research on the development of drug carriers is still active because issues such as a premature drug-release nonspecific delivery mechanism, unfavorable pharmacokinetics and biodistribution leading to unwanted side effects, and inefficient uptake at targeted sites that leads to low drug efficacy have to be solved.[1,8−10]

Aerogel is a type of intriguing porous material prepared by replacing the liquid solvent in a gel with air without substantially altering of the gel network.[16−18] These materials are composed of a network of interconnected nanostructures

Received: July 7, 2014
Accepted: August 18, 2014
Published: August 18, 2014

Scheme 1. Illustration of the Preparation Process Involved in ALS Aerogel Microspheres

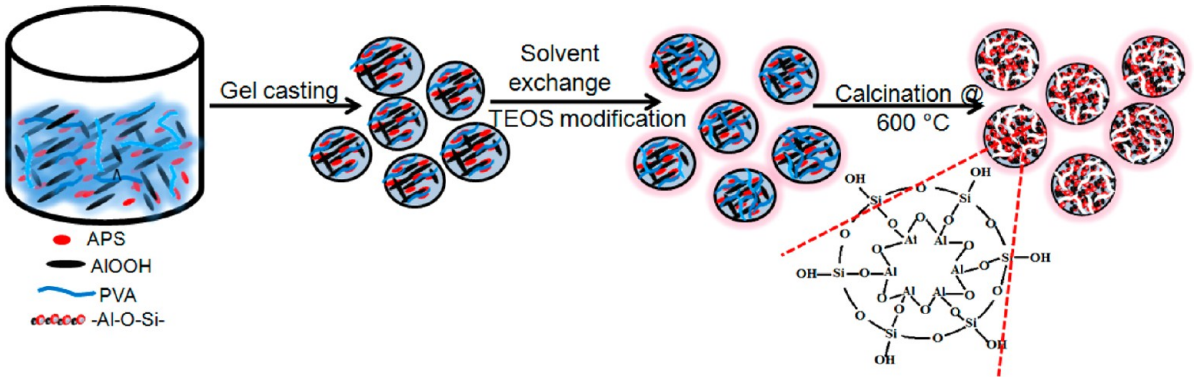

that exhibit high surface area, low density, and high porosity. The unique nature of aerogels is their multidimensional porosity in which macro/meso/micropores can be tailored by tuning the drying conditions. Silica aerogels having hydrophilic and hydrophobic surface properties have been investigated as DDSs for several pharmaceutically active compounds.[18−20] Silica aerogels improved the solubility of poorly soluble active drugs such as furosemide sodium,[19] griseofulvin,[20,21] ketoprofen,[20,22] penbutulol hemisulfate,[19] methylprednisolone,[19] miconazole,[22] etc., and their dissolution rate in aqueous solution. Silica-based aerogels are physically fragile, and in most of the earlier works, the drug-delivery studies are conducted in the powdery form.[19−22] One practical limitation observed in silica aerogel drug carriers is the fast penetration of liquid inside the aerogel, which resulted in disintegration of the aerogel structure, making it unsuitable for prolonged release. It is evident from the literature that, in silica-based aerogel systems, the drug-release rate is faster and about 80% of the drug is released within the first few minutes.[20] Moreover, a silica-based system (aerogel, ordered mesoporous silicates) undergoes degradation to silicic acid under physiological conditions. This can diffuse through the bloodstream and nucleate, causing adverse effects by the accumulation of fine particles in the body.[23,24]

Hybrid metal oxide−aerogel systems can overcome most of the critical issues associated with single-component silica aerogels. The drug loading and its delivery has not been studied and reported in such a hybrid aerogel matrix. Herein, we designed a hybrid system of aluminosiloxane (ALS) aerogel microspheres via a sol−gel route following a subcritical drying method by avoiding a risky and expensive supercritical drying process. The introduction of an ALS (Al−O−Si) network can strongly inhibit degradation, allow the self-limitation of soluble silica, and improve the mechanical integrity of the aerogel network. The ALS aerogel microspheres with an Al−O−Si framework exhibited a mesochanneled network of hierarchically porous architecture. A multidimensional hierarchically porous architecture not only enables high surface areas and high chemical activity sites but also enhances the mass transport of molecules and ions efficiently with fast diffusion to and from the active sites within the system.[25−27] This would be beneficial in DDSs for drug diffusion, which will increase the drug-loading and -release rates.

In this work, we have reported the influence of a hierarchically porous architecture, possessing mesochannels with multidimensional porosity, on the drug-delivery property. It is for the first time that an aerogel microsphere of the Al−O−Si framework with hierarchical porosity is under study for the drug-delivery property. Herein, we selected aspirin (ASP) and ibuprofen (IBU) as the model drugs having good pharmacological activity, which possess smaller and bigger molecular size, respectively, for the studies.[28,29] Comparative evaluation of the aerogel with ordered mesoporous MCM-41 was also performed and reported. In order to increase the positive charge density and drug uptake capacity, the surface of the aerogel is modified with APS. Thus, the carboxyl groups of the drug molecules can well interact with the surface hydroxyl groups or amino groups on the pore walls and can be useful for the controlled drug release. In vitro drug-release studies established a pH-triggered controlled-drug-release profile. In addition, various kinetic models were used to study the drug-release profile. Meanwhile, the resultant samples were well characterized by means of X-ray diffraction (XRD), Fourier transform infrared (FTIR), scanning electron microscopy (SEM), transmission electron microscopy (TEM), nitrogen adsorption/desorption measurements, ξ-potential measurements, and UV−vis spectroscopy. Furthermore, the biocompatibility of ALS aerogels with and without modification was checked via both ex vivo and in vivo studies.

2. EXPERIMENTAL SECTION

2.1. Materials and Reagents. Aluminum isopropoxide (AIP; purity >98%), (3-aminopropyl)trimethoxysilane (APS; purity >99%), and tetraethylorthosilicate (TEOS; purity >98%) were purchased from Aldrich and used as-received. Poly(vinyl alcohol) (PVA), ammonia solution (~25%), and paraffin liquid light were obtained from Merck Specialties Pvt. Ltd. Isopropyl alcohol, hexane, methanol, and nitric acid were purchased from Fisher Scientific. Aspirin (ASP; acetylsalicylic acid, 99%) and ibuprofen (IBU; 4-isobutyl-α-methylphenylacetic acid, 99%) were obtained from Alfa Aesar. All materials were used as obtained without further purification.

2.2. Preparation of Aluminosiloxane (ALS) Aerogel Microspheres. Alumina sol was prepared via a sol−gel route as per the procedure reported earlier by Yoldas.[30] In a typical procedure, 1 M AIP in 1000 mL of distilled water was stirred mechanically for 1 h at 80 °C. It was further stabilized at pH 3 through peptization using 0.7 M HNO_3. The peptized AIP sol was then refluxed at 80−85 °C for 48 h to form a stable hydrolyzed alumina sol. The Al_2O_3 content was gravimetrically estimated to be 0.0725 g mL^{-1}. A total of 56 mL (4 g of Al_2O_3) of alumina sol was homogenized mechanically with 10 mL of 0.5 wt % PVA for 30 min at 30 °C. Because both alumina sol and PVA possess hydroxyl groups, PVA appears to be a good choice as the binder. Hybrid alumina gel was then obtained by introducing different amounts in the APS/Al molar ratios of 0.1, 0.2, 0.4, 0.6, and 0.8. The APS addition suddenly increased the gel pH to >7. Therefore, H^+ ion (0.7 M HNO_3) was again added to compensate for the surplus counterions. A secondary introduction of acid increased the lowered surface potential of the gel and produced clear transparent sol at pH 3.

dx.doi.org/10.1021/am504422z | ACS Appl. Mater. Interfaces 2014, 6, 15564−15574

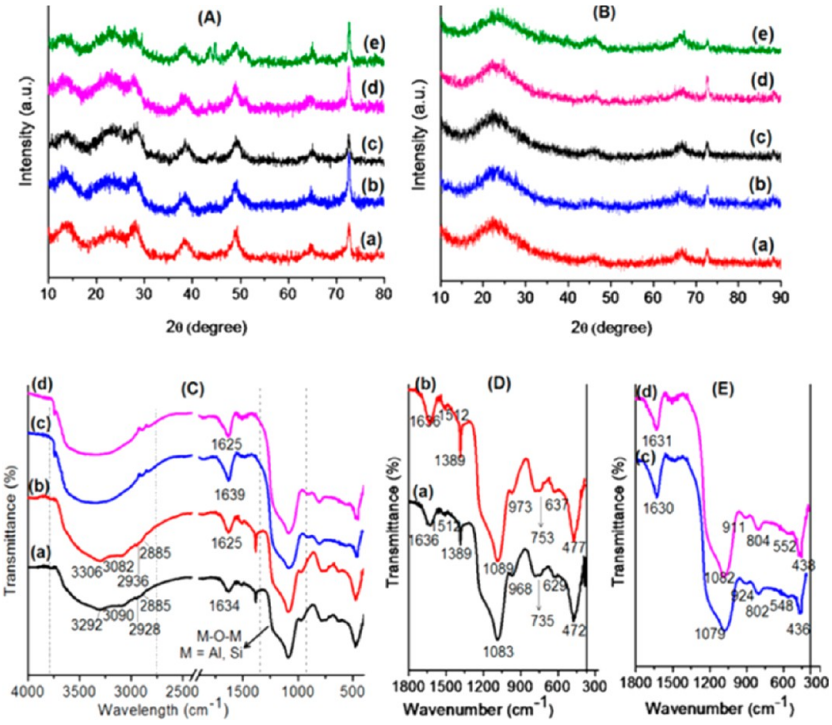

Figure 1. WAXS patterns of (A) as-dried and (B) calcined aerogel samples: (a) ALS0.1; (b) ALS0.2; (c) ALS0.4; (d) ALS0.6; (e) ALS0.8. FTIR spectra (C–E) were (a and b) as-dried ALS0.1 and ALS0.8 and (c and d) calcined ALS0.1 and ALS0.8, respectively.

Upon aging at room temperature, the sol became a flowable gel within seconds.

The gel was then injected into a chemical bath of an ammonia/paraffin oil mixture. Self-assembly of the gel in the oil layer forms well-defined microspheres because of surface tension. The wet gel microspheres thus obtained were washed with water and aged in isopropyl alcohol at 50 °C/24 h. After washing, solvent exchange with isopropyl alcohol was followed at least five times within 24 h so as to remove the liquid from the pores. Aging in a TEOS/hexane solution was followed for 48 h at 50 °C after solvent exchange. Excess TEOS from the surface was removed by washing with isopropyl alcohol. The experimental setup involving controlled drying by a "subcritical route" via solvent exchange, and surface modification is followed for the preparation of aerogel. Thus, multiple washing and solvent exchange steps were important to minimize the thermal stress during drying. In order to completely remove the occluded pore liquid from inside the gel network as well as on the surface, the microspheres were dried at 50 °C at ambient pressure, which resulted in stable aerogel microspheres. The dried aerogels were finally calcined to 600 °C for 2 h.

The aerogel samples were designated as ALS0.1, ALS0.2, ALS0.4, ALS0.6, and ALS0.8 based on the APS/Al ratio in the gel composition. Scheme 1 depicts a graphic for the preparation of ALS aerogel microspheres.

2.3. Surface Modification of ALS Aerogel Microspheres. Surface modification of aerogel microspheres was carried out by refluxing 1 g of ALS*x* samples with 2, 4, and 8 mmol of APS in dry toluene at 120 °C for 24 h. The resultant solid was filtered off, washed with toluene, and dried under a vacuum oven at 100 °C. These samples are referred to as ALS*x*-2NH, ALS*x*-4NH, and ALS*x*-8NH with respect to the lower and higher APS concentrations, respectively.

2.4. Loading and Release of the Drug. Two nonsteroidal antiinflammatory drugs, IBU and ASP, were selected for the experiment. For the drug-loading experiment, 60 mg samples were added into 25 mL of a 2 mg mL^{-1} IBU solution in hexane or 25 mL of 1 mg mL^{-1} ASP in methanol at room temperature. The sample flasks were sealed to prevent evaporation of the solvent, and then the mixture was shaken for 48 h. The sample was filtered and dried under a vacuum at 60 °C. The filtrate of IBU or ASP in solution was extracted from the flask and analyzed by measuring the UV–vis absorbance at 264 or 296 nm, respectively.

In vitro release experiments were performed in simulated gastric fluid (pH 2) and intestinal fluid (pH 7.4). Drug-loaded samples (about 0.2 g) were introduced to the corresponding drug-release medium (100 mL) in a conical flask at 37 °C, and the mixture was shaken continuously. At a given time, an aliquot of the solution was carefully removed for measurement of the released drugs in the solution. The content of IBU or ASP in solution was measured by UV–vis spectroscopy.

2.5. Biocompatibility Test. For biocompatibility testing, ex vivo and in vivo studies were performed. The ex vivo cell viability assay of ALS*x* samples was performed using a normal cell line (H9c2, immortalized ventricular myoblasts from rat embryo). In vivo studies of rat gastric ulceration were conducted to prove gastric protection of the material via the "pyloric ligation ulcer model". [More technical details of ex vivo and in vivo studies are provided in S1 in the Supporting Information (SI)]. An in vivo animal study was approved by the Institutional Animal Ethical Committee (IAEC), Department of Pharmacology, K. M. College of Pharmacy, Tamilnadu, India, under ethical committee file no. *TALASILA SINDHOOR/M.Pharm/261210108/IAEC/KMCP/114/2013–2014*.

2.6. Characterization Techniques. The physical, chemical, and surface properties of the ALS*x* aerogel microspheres processed in the present work were systematically characterized using several instrumental techniques. Wide-angle XRD (WAXS) patterns were obtained with a Philips X'pertPro diffractometer in the 2θ range 10–90° using Cu Kα radiation (λ = 1.54178 Å). Small-angle XRD (SAXS) patterns were recorded on a Xeuss-SAXS/WAXS system by Xenocs equipped with Cu Kα radiation (λ = 0.1540 nm). Structural analysis of the samples was performed by a FTIR spectrophotometer (IR Prestige-21, Shimadzu) in the wavelength range 4000–400 cm^{-1} using a KBr pellet technique in transmittance mode. The microstructures of the aerogels were examined using a ZEISS EVO 18 Special Edition scanning electron microscope, operated at 20 kV. TEM images were recorded using a FEI Tecnai 30G2S- TWIN transmission electron microscope operated at an accelerating voltage of 300 kV. Nitrogen adsorption/desorption isotherm measurements of the aerogel samples were performed with a Micromeritics Gemini 2375 instrument. All of

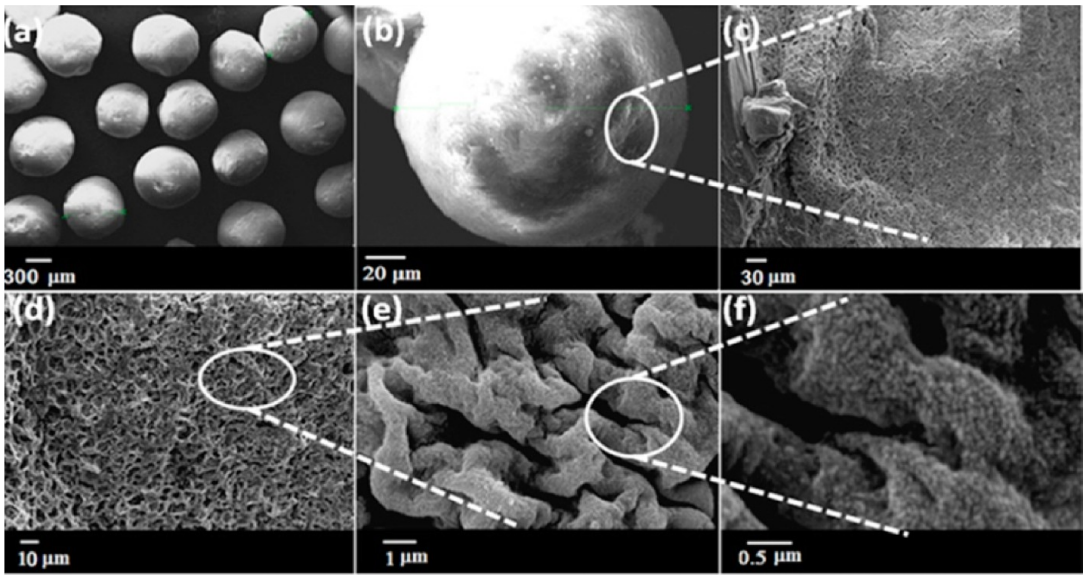

Figure 2. (a–f) SEM images of the hierarchically porous ALS aerogel microspheres at different magnifications to probe the macro- and mesoporous properties.

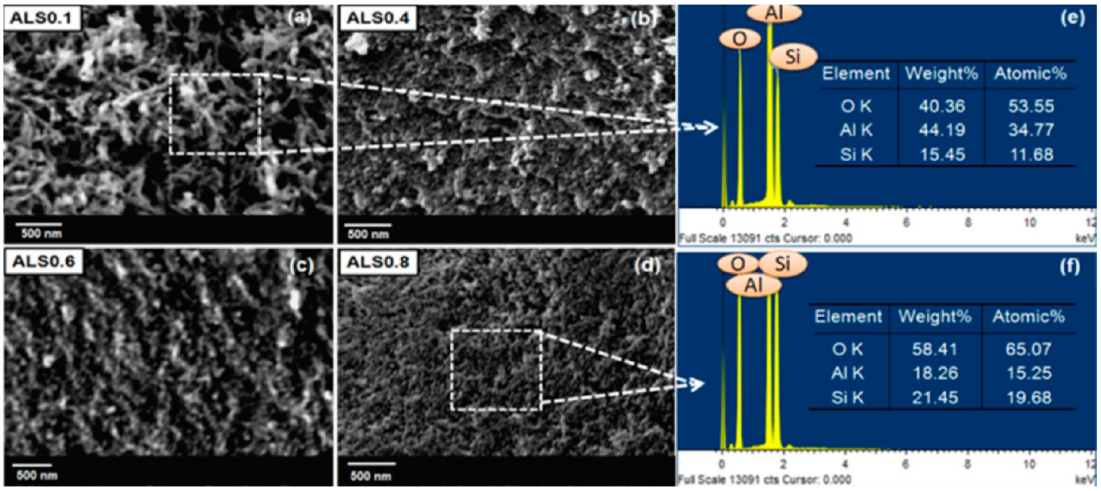

Figure 3. (a–d) SEM (high magnification 50.00KX) images of the different compositions of ALS aerogels. (e and f) EDX pattern of two extreme compositions of ALS samples.

the aerogel samples were degassed at 200 °C for 2 h, and the functionalized samples were degassed at 100 °C for 2 h under a nitrogen atmosphere prior to adsorption measurements. The Brunauer–Emmett–Teller (BET) model was utilized to calculate the specific surface areas. A desorption isotherm was used to determine the pore-size distribution using the Barrett–Joyner–Halenda (BJH) model. The porosity and true density of the aerogel samples were calculated by the "density bottle method" using water or ethanol as the medium to fill the pores.[31] UV–vis spectra were recorded on a Shimadzu UV-2450 spectrophotometer.

3. RESULTS AND DISCUSSION

3.1. Structural and Textural Analysis of ALS Aerogel Microspheres. Parts A and B of Figure 1 show the WAXS patterns of the as-dried and calcined ALS samples with respect to the APS/Al molar ratios. The WAXS patterns taken on a pure alumina aerogel at low temperatures have shown peaks at 2θ = 14°, 28°, 38°, and 49°, confirming the presence of a boehmite phase.[32,33] In as-dried ALS aerogels for lower APS/Al molar ratios, the boehmite peak intensity is high, decreasing when the amount of APS is increased.

Moreover, broad and comparatively weak peaks are noticed at 2θ between 22 and 27° with increasing APS. These peaks clearly suggest that the as-dried ALS aerogel matrix has predominantly semicrystalline hydroxy alumina and silica phases. In calcined ALS aerogels, the WAXS pattern showed three very weak and broad peaks at 2θ values of 22°, 45°, and 66° corresponding to a lower degree of crystallinity. From XRD results, we confirmed that the molecular-scale mixing of two metal oxide precursors inhibited the preferential crystalline growth of any transition alumina during calcination and resulted in noncrystalline Al–O–Si frameworks.

Parts C–E of Figure 1 show the FTIR spectra of as-dried [(a) ALS0.1 and (b) ALS0.8] and calcined [(c) ALS0.1 and (d) ALS0.8] aerogel samples. An intense broad band (full width at half-maximum of 237 cm^{-1} for part a and 230 cm^{-1} for part b) with peaks at 3292 and 3090 cm^{-1} and 3306 and 3082 cm^{-1} assigned to the –OH groups of Al–OH and Si–OH for parts a and b, respectively. The bands at 2928 and 2885 cm^{-1} and 2936

dx.doi.org/10.1021/am504422z | ACS Appl. Mater. Interfaces 2014, 6, 15564–15574

and 2885 cm^{-1} are assigned to C−H symmetric and asymmetric stretching vibrations in parts a and b, respectively. These absorption bands are found to disappear after calcination. For more clarity on the important metal oxygen (M−O) vibrations appearing in the region 1800−400 cm^{-1},[34] the spectrum of this region is shown separately for as-dried and calcined aerogels in parts C and D of Figure 1, respectively. The broad adsorption in the range 1200−950 cm^{-1} indicates the stretching vibration of Al−O−Si and Si−O−Si bonds.[35] Generally, aluminum can have different types of coordinations with oxygen, either octahedral (AlO_6) or tetrahedral (AlO_4). The stretching and bending modes of an AlO_6 moiety are expected in the regions 500−750 and 330−450 cm^{-1}, respectively, while for AlO_4, they appear in the regions 750−850 and 250−320 cm^{-1}, respectively.[36,37] The observed frequencies for ALS samples are listed in Table S1 in the SI. In the observed spectrum, peaks at 735, 629, and 472 cm^{-1} for part a and 753, 637, and 477 cm^{-1} for part b are assigned to the stretching and bending modes of only AlO_6. The bands are shifted to higher frequencies for higher amounts of a silicon-containing sample. In the spectra of calcined samples, 802, 552, and 438 cm^{-1} for part c and 804, 552, and 438 cm^{-1} for part d are assigned to the stretching mode of both AlO_4 and AlO_6. Thus, the formation of tetrahedral along with octahedral coordination sites in calcined samples is evident from the FTIR spectrum.

The skeletal frameworks of the ALS aerogel were observed via electron microscopy. The micro- to nanostructure of the aerogel microsphere is depicted in various magnifications of SEM images in Figure 2a−f. Images clearly describe the various levels of porosity in the system ranging from macropores to mesopores. A periodical arrangement of well-connected macroporous walls with pore sizes in the range 0.5−1 μm can be seen. Higher magnification (50.00KX) SEM images in Figure 3a−d further revealed that the macroporous wall contains a 3D interconnected mesopore network. As the silicon content in the samples increased, a notable variation in the surface morphology with a gradual decrease in the porosity was observed. The porous skeleton changes from a fragmented cocontinuous structure (ALS0.1) to a more homogeneous cocontinuous porous skeleton with smoother skeleton surfaces (ALS0.8).

The elemental mapping was also carried out by energy-dispersive X-ray (EDX) analysis on ALS0.1 and ALS0.8 aerogels, and the results clearly show the presence of only aluminum, oxygen, and silicon elements in the aerogels (Figure 3e,f). From FTIR, WAXS, and EDX results, it is apparent that the calcined ALS aerogels processed from two metal oxide precursors possess a pure Al−O−Si framework having well-tuned structural hierarchy. In fact, the hierarchical nature was also very clearly seen in TEM images.

TEM images in Figure 4a,b show the interconnected network of nanometer-sized fibrous particles. The particle width increased from 5 to 10 nm in ALS0.1 and from 10 to 30 nm in ALS0.8. Interestingly, the formation of randomly oriented mesochannels was also visible in TEM images in Figure 4c−f. The tubular extension of mesopores can help in the interconnection of meso- and macropores in the system. The SAXS pattern of the samples showed a diffraction peak below $2\theta = 0.5°$, which also indicates the presence of interconnected mesopores (shown in Figure S1 in the SI).[38]

In order to further probe the porous nature of the aerogel network, nitrogen adsorption/desorption isotherms and their

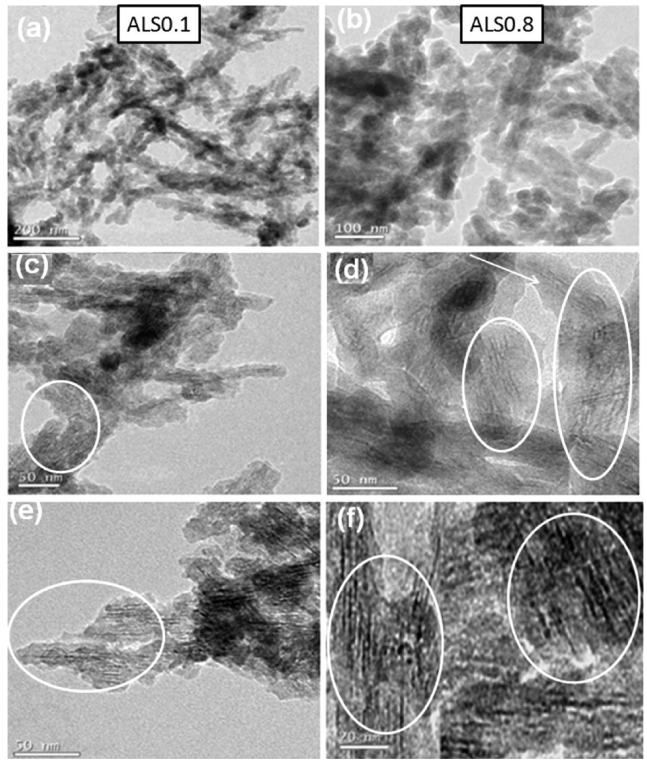

Figure 4. TEM images of ALS0.1 and ALS0.8 at various magnifications (a−f) indicating an interconnected network with mesochannels.

pore-size distributions are acquired, and the results are presented in parts A and B of Figure 5, respectively. This explains that the isotherms (Figure 5A) corresponding to all aerogel samples resemble a combination of type IV and II isotherms. It was seen that the adsorption and desorption isotherms in $0.05 \leq p/p^0 \leq 0.7$ overlapped each other because of the formation of monolayer and multilayer adsorption behavior. Moreover, the formation of a hysteresis loop in the isotherm suggests the presence of mesopores in all samples. At $p/p^0 > 0.8$, the adsorbed volume of nitrogen rises very steeply at high relative pressure, which suggests the presence of an appreciable amount of secondary porosity of very large mesopores and macropores.[39] The hysteresis loops of the adsorption/desorption isotherms have a combination of H1 and H3 character, indicating that these samples are comprised of loose assemblages of particles corresponding to cylindrical and slit-shape pore geometries.[40] From the BJH pore-size distribution curve in Figure 5B, a typical hierarchical size of the mesopores and macropores is noticed.

A summary of the physical properties such as shrinkage, bulk density, and porosity along with the results from BET measurements of all of the ALS samples is presented in Table 1. All of these parameters, excluding the bulk density, showed a decreasing trend with increasing silicon content in ALS samples. The shrinkage could be minimized from ∼85% (for xerogel samples obtained by evaporative drying) to ∼15% in ALS aerogels. Similarly, the bulk density varied in the range 0.292−0.355 g cm^{-3} with increasing silicon content. The BET/Langmuir surface area ranges from 371/569 to 269/387 m^2 g^{-1}. The results suggest that porous hierarchy can be tailored to different lengths integrated in one solid body by fine-tuning the self-assembly of AlOOH and APS at various ratios.

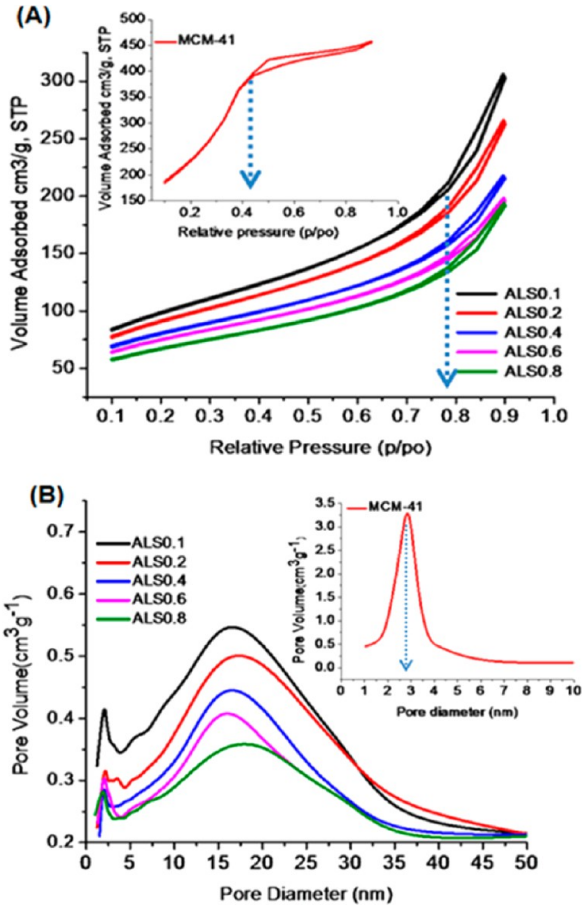

Figure 5. (A) Nitrogen adsorption/desorption isotherms. (B) BJH pore-size distributions of ALS aerogel samples. The corresponding insets show curves of the 1D porous system MCM-41.

Encouraged by the hierarchically porous framework in ALS aerogel microspheres, we have explored the potential application of our new materials for designing DDSs. Ordered mesoporous materials with novel pore properties have been shown to be excellent candidates for local DDSs in biomedical applications.[9−15] Hence, we have made a comparative study of ALS with one of the most well-studied ordered mesoporous material MCM-41. The pore features of MCM-41 used in this study are shown along with the results of ALS aerogels in the inset of Figure 5A,B and Table 1, which ensures that it as a typical mesoporous material with monomodel pores and high surface area.

3.2. Drug-Loading and -Release Studies in ALS Aerogel Microspheres. *3.2.1. Loading of IBU and ASP.* To evaluate the capability of ALS aerogels as DDSs, IBU and ASP were entrapped in "multidimensional nanoporous reservoirs" of an aerogel framework. Table 2 displays the

Table 2. Amounts of Drug Loading in ALS Aerogels and MCM-41 Analyzed by UV−Vis Spectroscopy

unmodified sample	loading of mg of IBU per g of sample	loading of mg of ASP per g of sample	APS-modified aample	loading of mg of IBU per g of sample	loading of mg of ASP per g of sample
ALS0.1	567	108	AL0.5S-1NH	595	
ALS0.2	536	180	AL0.5S-2NH	640	
ALS0.4	530	198	AL0.5S-3NH	365	
ALS0.6	515	231	AL4S-1NH		287
ALS0.8	495	273	AL4S-2NH		301
MCM-41 (present work)	359	213	AL4S-3NH		143
MCM-41 (literature report)	337,[7] 230[28]	100[29]			

adsorption capacities of the model drugs, in hierarchically porous ALS aerogel and single-model mesoporous MCM-41. It was seen that MCM-41 could load maxima of 359 mg g^{-1} of IBU and 213 mg g^{-1} of ASP, which falls in line with the previous reports,[7,28,29] while a maximum of 567 mg g^{-1} of IBU was loaded in ALS0.1 and that of 273 mg g^{-1} of ASP was loaded in ALS0.8, indicating a high loading capacity of ALS aerogel samples. The loading capacity is mainly related to adsorption and diffusion of a drug to the active sites, as depicted in Scheme 2. When drug molecules diffuse through the long tubular and 1D mesopores of MCM-41, there is chance of drug to be clogged up at the entrance. This leads to a low drug loading in mesochannels of MCM-41, even though it is having high surface area. While the hierarchically meso and macropores of aerogel reduce resistance to diffusion of drug molecules and improves the mass transport through macropores for penetration of the drug into inner short meso channels. This finally leads to large amount of drug loading in multiporous aerogel samples.

It was also seen that, along with the porosity of the material, the dimensions of drug molecules influence the drug-loading capacity. IBU with bigger molecular size (1 × 0.5 nm) and ASP with smaller molecular size (0.75 × 0.24 nm) showed

Table 1. Summary of the Physicochemical Properties of the Porous Samples

sample	shrinkage (%)[a]	bulk density (g cm^{-3})	porosity (%)	surface area BET/ Langmuir (m^2 g^{-1})[b]	mesopore volume (cm^3 g^{-1})[b]	total pore volume (cm^3 g^{-1})[b]	average pore diameter (2−10)/(10−50) (nm)[b]
ALS0.1	17 (86)	0.292	91	371/569	0.4815	0.5058	5.6/26.8
ALS0.2	16 (83)	0.314	90	342/521	0.4161	0.4339	5.4/26.4
ALS0.4	16 (82)	0.326	90	302/469	0.3734	0.3857	5.2/25.6
ALS0.6	14 (82)	0.324	89	284/418	0.3204	0.3316	4.8/25.1
ALS0.8	13 (81)	0.355	86	269/387	0.2963	0.3065	4.6/25.0
MCM-41				895/1027	0.7668	0.7668	2.8

[a]Shrinkage = 100(diameter of as-synthesized samples) − (diameter after drying)/(diameter of as-synthesized samples). For shrinkage data for the corresponding xerogel samples obtained by evaporative drying shown in parentheses. [b]Results obtained from BET measurements.

Scheme 2. Schematic Representation of the Drug-Loading Process in (a) MCM-41 and (b) ALS Aerogel Microspheres

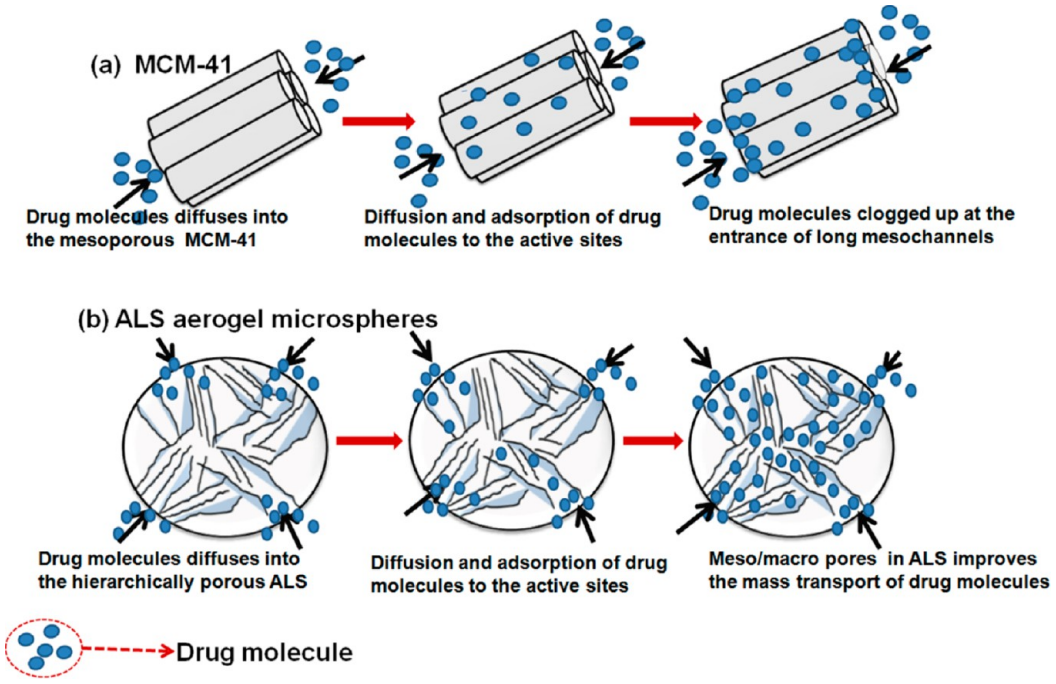

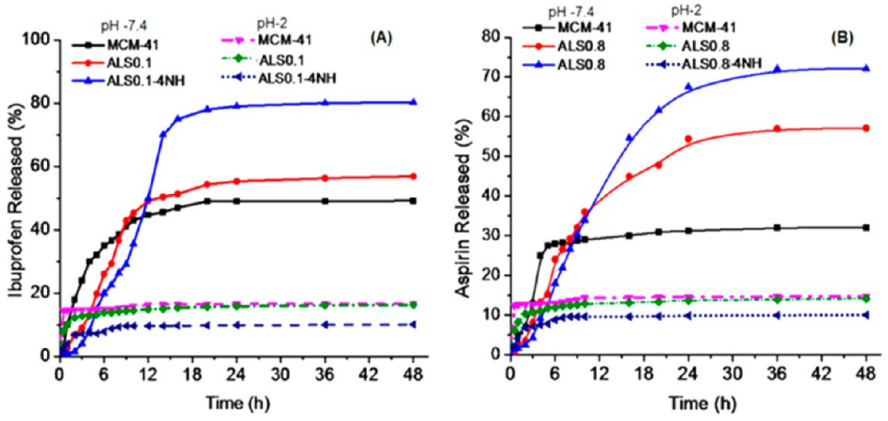

Figure 6. In vitro release profile of (A) IBU- and (B) ASP-loaded ALS aerogels and MCM-41 under different pH solutions (pH 7.4 and 2).

maximum loading in higher- and lower-pore-size ALS systems, respectively (Table 2). Thus, the drug adsorption behavior governed by the "size selectivity of host/guest", i.e., pore size, pore connectivity, and pore geometry, influences the size of the guest drug molecule.

In order to incorporate a higher dosage of drug, we further modified the surface of ALS*x* with APS at three different compositions. A minimum amount of 4 mmol g^{-1} APS is required for enhancement in the loading of IBU from 567 to 640 mg g^{-1} for ALS0.1 and of ASP from 273 to 301 mg g^{-1} for ALS0.8 samples. When a maximum of 8 mmol g^{-1} APS was used for modification, the drug loading declined. This may possibly be due to blocking of the pore by excess APS. So, the higher loading of drugs in APS-modified samples is attributed to the favorable interaction of the amine group with the carboxyl group present in the drug molecules.

3.2.2. In Vitro Release Studies. To design a good DDS, not only is it necessary to incorporate a maximum amount of drug, but also slow and controlled release is equally important. The drug-release profiles for maximum-drug-loaded ALS samples and MCM-41 were obtained from the results of in vitro studies. Figure 6A shows the release behavior of IBU and Figure 6B that of ASP for selected samples in simulated body fluids of pH 2 and 7.4 over a period of 48 h. About 30−45% of the loaded drug was released from the pores of MCM-41, while a maximum of 70−80% of the loaded drug was released from ALS aerogel at pH 7.4. It is seen that, at pH 7.4, MCM-41 exhibited a higher initial burst release of 35% of loaded IBU within the initial 5 h, while ALS0.1 and ALS0.1−4NH showed only 19% and 15% release, respectively, in 5 h (Figure 7a). Similarly, MCM-41 showed about 27% ASP release at pH 7.4; however, only 15% and 11% release was shown for ALS0.8 and ALS0.8−4NH, respectively, in 5 h (Figure. 7c). In addition, the release profile for the samples in simulated fluid at pH 2 showed insignificant release not only in the initial burst release for MCM-41 but also for ALS samples when followed up to 5 h (Figure 7b,d). Further, amine-modified ALS (ALS0.1−4NH and ALS0.8−4NH) still showed lower release rates at pH 2.

Variation in the release rates of these samples could be explained from the discrepancy of the surface charge of the

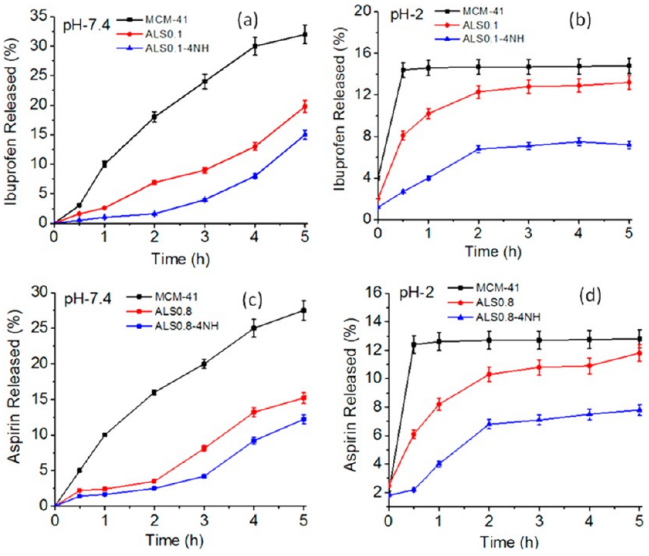

Figure 7. Initial 5 h release profile (a) and (b) IBU loaded samples, (c) and (d) ASP loaded samples at pH 7.4 and pH 2 respectively.

samples in different pH solutions.[41−44] At pH 2.0, all of the samples showed positive ξ-potential values, even in amine-modified ALS (ALS0.1, +12.6; ALS0.8, +3.7; ALS0.1−4NH, +30.5; ALS0.8−4NH, +21.5; MCM-41, +2.6 mV). When the pH was raised to 7.4, all samples exhibited negative ξ-potential values (ALS0.1, −15.1; ALS0.8, −34.4; ALS0.1−4NH, −11.7; ALS0.8−4NH, −25.7; MCM-41, −40.4 mV). Thus, at pH 7.4, the surface became deprotonated, and a strong electrostatic repulsion between the negative charge of the sample (Al−O^- or Si−O^-) and the negative charge of the drug molecules (−COO^-) (both IBU and ASP) was generated. Consequently, the release rate of the drug molecules will be promoted at this pH and is even more enhanced in amine-modified ALS samples, while in acidic conditions, samples showed a decrease in the release rate due to the electrostatic attraction between the positively charged sample and negatively charged drug molecules. For amine-modified ALS, the amount of protonated species (−NH_3^+) is more dominant because of the strong electrostatic attraction between −NH_3^+ and $^-$OOC−, showing a relatively lower release, while in the case of MCM-41, the positive charge density is lower at pH 2, which resulted in a burst release compared to ALS samples (Figure 7b,d).

The release profile was also applied on various kinetic models in order to find the mechanism of drug release (models used and corresponding equation given in Table S2 in the SI). The kinetic modeling of release profiles was carried out using Systat Software, Inc. *Sigma Plot 12.0* using the controlled-release extension library file. The models were fitted to the initial 5 h of the drug-release profile considering the average gastric retention time where drug release exponentially increases and then later attains a constant rate. The parameters obtained after fitting release data are listed in Table 3. The drug-release kinetics falls in line with zero-order, as indicated by the R^2 value of ≥0.9 for ALS samples, proving the drug release from the pores in a controlled manner. The release was also found to be independent of the concentration of drug remaining in the pores. MCM-41 was fitted to first-order kinetics, which accounts for burst release. Because the ALS samples follow zero-order kinetics, the study was extended to realize the dynamics of drug release. Both Higuchi and Korsmeyer−Peppas models were used to obtain the possible release mechanism. The release charactersistics of ALS samples were best fitted with the Korsmeyer−Peppas model, with an n value in the range 0.4634−0.5609 indicating that diffusion was the predominant mechanism of drug release. MCM-41 fits well in the Higuchi model compared to ALS samples, as observed in earlier reports.[29] For ALS samples, k values fall in the range for a controlled-release carrier, while MCM-41 showed higher k values than those required for controlled release. Thus, the release pattern from the kinetic modeling studies showed that the drug releases with a zero-order kinetics following the Korsmeyer−Peppas model, proving ALS aerogel as a controlled DDS.

An integrated graphical plot of the maximum drug molecules loaded and released from single-sized mesoporous MCM-41 and hierarchically porous ALS aerogel is presented in Figure 8. This clearly shows that the loading ability of a hierarchically porous system is far higher than that of a single-sized porous system. Similarly, the hierarchical system exhibited release of more than 50% the loaded drug molecules, while MCM-41 showed only a meager release of the loaded drug. Thus, ALS aerogels could be a good choice as drug carriers for biomedical applications.

The basic and preliminary criterion for biomedical application of new kinds of materials is its biocompatibility. Therefore, in order to investigate the cytotoxicity/biocompatibility level of ALS aerogels, ex vivo and in vivo studies were preformed, and the results are shown in Figure 9. In order to investigate the cytotoxicity level of ALS and ALS-NH aerogel microspheres, an ex vivo test was carried out by MTT assay in normal H9c2 cell lines (immortalized ventricular myoblasts from rat embryo; a further description is given in S1.1a and S1.1b in the SI) . Results in Figure 9A show 500 μg $well^{-1}$ of ALS; ALS-NH aerogels were highly viable for H9c2 cell lines.

A modified pyloric ligation ulceration test was performed to prove the biosafety of ALS aerogels by in vivo analysis. Gastric ulceration was induced in albino male rats with a pure ASP

Table 3. Properties of the Kinetic Model Parameters for Drug-Release Studies at pH 7.4

		kinetic models and related parameters						
				Higuchi		Korsmeyer−Peppas		
drug release	sample	zero-order R^2	first-order R^2	R^2	k	R^2	n	k
IBU	ALS0.1	0.9924	0.9731	0.7949	10.4543	0.9914	0.4634	11.6529
	ALS0.1−4NH	0.9815	0.894	0.6781	13.2298	0.9847	0.5188	9.2644
	MCM-41	0.9076	0.9347	0.9799	10.4178	0.9654	0.2961	18.9154
ASP	ALS0.8	0.98406	0.9477	0.7681	9.5279	0.9851	0.5266	8.8073
	ALS0.8−4NH	0.98607	0.9089	0.7046	10.985	0.9936	0.5609	8.8072
	MCM-41	0.88421	0.9578	0.9525	6.9008	0.9173	0.4047	10.8075

dx.doi.org/10.1021/am504422z | *ACS Appl. Mater. Interfaces* 2014, 6, 15564−15574

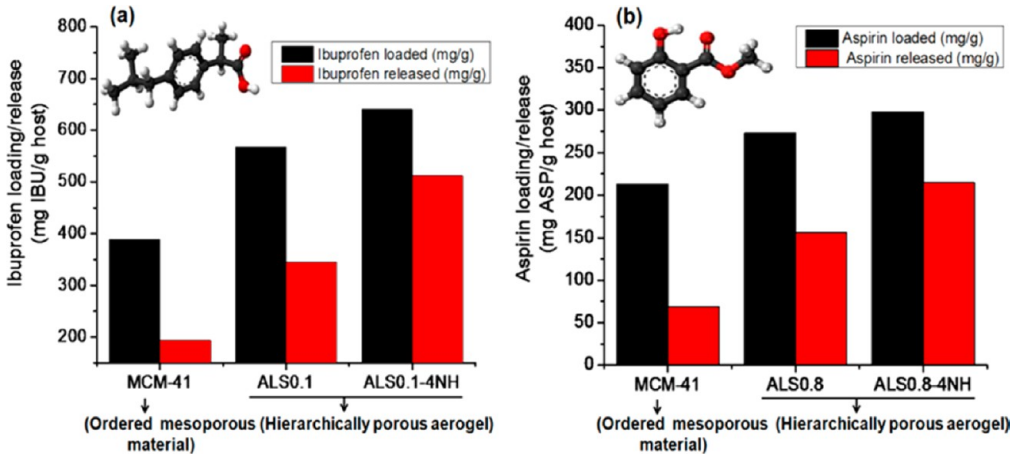

Figure 8. (a) IBU and (b) ASP loading (black) and release (red) from ALS aerogels and MCM-41 samples.

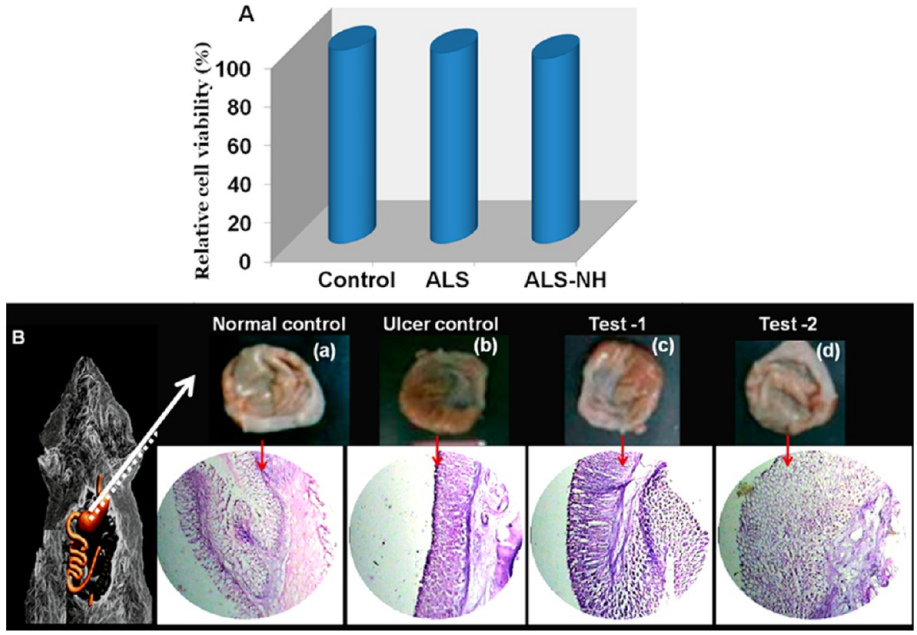

Figure 9. Ex vivo (A) and in vivo (B) studies performed to check the cytotoxicity/biocompatibility of the ALS material.

drug. Hence, ASP-loaded ALS aerogel microspheres (ASP-ALS and ASP-ALS-NH) were chosen as the test samples (elaborated on in S1.2 in the SI). After test days, animals were subjected to histopathological studies. Photographic images and corresponding histopathological slides of gastric pylorus of (a) normal control, (b) ulcer control, (c) Test-1, and (d) Test-2 are shown in Figure 9B. Results analyzed from the histopathology slides proved that in part a the epithelial mucous layer and the cells within are intact, while an ulcer-induced set (b) shows strong infiltration by inflammatory cells fibroblasts and endothelial cells, indicating complete disruption of the gastric epithelial layer. Test-1 and Test-2 of animal dissections given with test samples replicated a healthy shape of the epithelial mucosa as in normal control promising the biocompatibility of the carrier. The healthy epithelial layer also assures that no drug is released at acidic gastric pH from ALS samples. In vivo analysis of gastric pylorus thus confirmed the pH-responsive drug-release capability of ASL aerogels, as evidenced in the in vitro release profile.

A futuristic outlook can be envisaged by utilizing these ALS aerogel microspheres in potential bone tissue engineering for defect filling and regeneration. Therefore, the bioactive ALS aerogels can be an attractive and innovative solution for enhancing bone tissue growth rate, thereby improving mechanical bone fixation and thus leading to enhancement in the lifetime of implants. The property of controlled drug release can be utilized in delivering antiinfective drugs that can be well entrapped on the fillers. Thus, it can act as potential therapeutic bone fillers at the time of surgery, as illustrated in Scheme 3.

4. CONCLUSIONS

In summary, an efficient aerogel framework of ALS microspheres was developed by sol−gel-assisted cocondensation of hydrolyzed alumina (AlOOH) and APS. The hybrid metal oxide aerogel of an Al−O−Si skeletal framework showed hierarchical porous architecture having mesochannels and provides mechanical strength to the aerogel network. A comparative study was performed to evaluate the drug-loading capacity and drug-release property of hierarchically porous system (ALS aerogels) with single-sized ordered mesoporous material (MCM-41) using IBU and ASP as a model drugs. The

Scheme 3. Schematic Illustration of a Possible Outlook of Hierarchically Porous Aerogel Microspheres

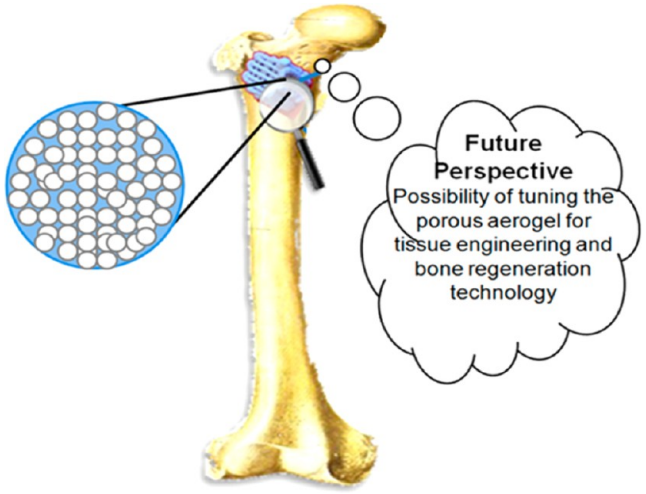

adsorption capacity and release behavior was found to be highly dependent on the porous architecture of the material. The multidimensional hierarchically porous structure in ALS aerogel microspheres enhanced the mass transport of drug molecules through macropores into inner short mesochannels, while long and 1D mesopores in MCM-41 hindered drug diffusion into the porous channels. As a result, ALS*x* and ALS*x*-4NH showed maximum loading amounts of 567 mg g^{-1} of IBU, 273 mg g^{-1} of ASP and 640 mg g^{-1} of IBU, 301 mg g^{-1} of ASP, respectively, whereas MCM-41 could load maxima of 359 mg g^{-1} of IBU and 213 mg g^{-1} of ASP. Variation in the surface charge of the ALS aerogel also showed a pH-responsive drug-release behavior. Kinetic modeling of the drug-release profile for ALS aerogels gave zero-order kinetics following the Korsmeyer–Peppas model, indicating a controlled DDS with diffusion as the predominant mechanism of drug release. We have also established the biocompatibility and lower toxicity level for ALS aerogel via ex vivo and in vivo studies marking the material inexpensive and a reasonable candidate for biomedical applications.

■ ASSOCIATED CONTENT

Supporting Information

Detailed experimental procedures of ex vivo and in vivo biocompatibility tests, vibrational transitions in the FTIR spectrum and SAXS pattern of ALS aerogel samples, and kinetic models used for analysis of drug-release data. This material is available free of charge via the Internet at http://pubs.acs.org.

■ AUTHOR INFORMATION

Corresponding Author

*E-mail: ananthakumar70@gmail.com. Tel.: 91-471-2515289 or +91-9497271547.

Notes

The authors declare no competing financial interest.

■ ACKNOWLEDGMENTS

The authors thank Dr. Suresh Das, Director, National Institute for Interdisciplinary Science & Technology, NIIST-CSIR, for providing laboratory facilities for the work. V.L. is grateful to the University Grants Commission (UGC), Government of India, for providing a Senior Research Fellowship to carry out this work. Mr. Kiran and Lucy Paul are acknowledged for TEM and SEM analysis, respectively. All of the members of the Materials Science and Technology Division are acknowledged for providing general support.

■ REFERENCES

(1) Arruebo, M. Drug Delivery from Structured Porous Inorganic Materials. *Wiley Interdiscip. Rev.: Nanomed. Nanobiotechnol.* **2012**, *4*, 16–30.
(2) Kwon, S.; Singh, R. K.; Perez, R. A.; Abou Neel, E. A.; Kim, H.-W.; Chrzanowski, W. Silica-Based Mesoporous Nanoparticles for Controlled Drug Delivery. *J. Tissue Eng.* **2013**, *4*, 2041731413503357.
(3) Larson, N.; Ghandehari, H. Polymeric Conjugates for Drug Delivery. *Chem. Mater.* **2012**, *24*, 840–853.
(4) Kumari, A.; Yadav, S. K.; Yadav, S. C. Biodegradable Polymeric Nanoparticles Based Drug Delivery Systems. *Colloids Surf., B* **2010**, *75*, 1–18.
(5) Zhang, L.; Chan, J. M.; Gu, F. X.; Rhee, J.-W.; Wang, A. Z.; Radovic-Moreno, A. F.; Alexis, F.; Langer, R.; Farokhzad, O. C. Self-Assembled Lipid–Polymer Hybrid Nanoparticles: A Robust Drug Delivery Platform. *ACS Nano* **2008**, *2*, 1696–1702.
(6) Vallet-Regi, M. Ordered Mesoporous Materials in the Context of Drug Delivery Systems and Bone Tissue Engineering. *Chem.—Eur. J.* **2006**, *12*, 5934–5943.
(7) Manzano, M.; Vallet-Regi, M. New Developments in Ordered Mesoporous Materials for Drug Delivery. *J. Mater. Chem.* **2010**, *20*, 5593–5604.
(8) Horcajada, P.; Serre, C.; Maurin, G.; Ramsahye, N. A.; Balas, F.; Vallet-Regi, M.; Sebban, M.; Taulelle, F.; Ferey, G. Flexible Porous Metal–Organic Frameworks for a Controlled Drug Delivery. *J. Am. Chem. Soc.* **2008**, *130*, 6774–6780.
(9) Mai, W. X.; Meng, H. Mesoporous Silica Nanoparticles: A Multifunctional Nano Therapeutic System. *Integr. Biol.* **2013**, *5*, 19–28.
(10) Tang, F.; Li, L.; Chen, D. Mesoporous Silica Nanoparticles: Synthesis, Biocompatibility and Drug Delivery. *Adv. Mater.* **2012**, *24*, 1504–1534.
(11) Heikkila, T.; Salonen, J.; Tuura, J.; Kumar, N.; Salmi, T.; Murzin, D. Y.; Hamdy, M. S.; Mul, G.; Laitinen, L.; Kaukonen, A. M.; Hirvonen, J.; Lehto, V. P. Evaluation of Mesoporous TCPSi, MCM-41, SBA-15, and TUD-1 Materials as API Carriers for Oral Drug Delivery. *Drug Delivery* **2007**, *14*, 337–347.
(12) Zhang, L.; Qiao, S.; Jin, Y.; Cheng, L.; Yan, Z.; Lu, G. Q. Hydrophobic Functional Group Initiated Helical Mesostructured Silica for Controlled Drug Release. *Adv. Funct. Mater.* **2008**, *18*, 3834–3842.
(13) Yang, P.; Gai, S.; Lin, J. Functionalized Mesoporous Silica Materials for Controlled Drug Delivery. *Chem. Soc. Rev.* **2012**, *41*, 3679–3698.
(14) Lee, C.-H.; Lo, L.-W.; Mou, C.-Y.; Yang, C.-S. Synthesis and Characterization of Positive-Charge Functionalized Mesoporous Silica Nanoparticles for Oral Drug Delivery of an Anti-Inflammatory Drug. *Adv. Funct. Mater.* **2008**, *18*, 3283–3292.
(15) Tang, Q.; Xu, Y.; Wu, D.; Sun, Y.; Wang, J.; Xu, J.; Deng, F. Studies on a New Carrier of Trimethylsilyl-Modified Mesoporous Material for Controlled Drug Delivery. *J. Controlled Release* **2006**, *114*, 41–46.
(16) Husing, N.; Schubert, U. Aerogels Airy Materials: Chemistry, Structure, and Properties. *Angew. Chem., Int. Ed.* **1998**, *37*, 23–45.
(17) Du, A.; Zhou, B.; Zhang, Z.; Shen, J. A Special Material or a New State of Matter: A Review and Reconsideration of the Aerogel. *Materials* **2013**, *6*, 941–968.
(18) Ulker, Z.; Erkey, C. An Emerging Platform for Drug Delivery: Aerogel Based Systems. *J. Controlled Release* **2014**, *177*, 51–63.
(19) Schwertfeger, F.; Zimmerman, A.; KrempelH. Use of Inorganic Aerogels in Pharmacy. U.S. Patent 6,280,744, 2001.

(20) Smirnova, I.; Suttiruengwong, S.; Seiler, M.; Arlt, W. Dissolution Rate Enhancement by Adsorption of Poorly Soluble Drugs on Hydrophilic Silica Aerogels. *Pharm. Dev. Technol.* **2004**, *9*, 443−452.
(21) Smirnova, I.; Turk, M.; Wischumerski, R.; Wahl, M. A. Comparison of Different Methods for Enhancing the Dissolution Rate of Poorly Soluble Drugs: Case of Griseofulvin. *Eng. Life Sci.* **2005**, *5*, 277−280.
(22) Smirnova, I.; Mamic, J.; Arlt, W. Adsorption of Drugs on Silica Aerogels. *Langmuir* **2003**, *19*, 8521−8525.
(23) Fontecave, T.; Sanchez, C.; Azais, T.; Boissiere, C. Chemical Modification as a Versatile Tool for Tuning Stability of Silica Based Mesoporous Carriers in Biologically Relevant Conditions. *Chem. Mater.* **2012**, *24*, 4326−4336.
(24) Bang, A.; Sadekar, A. G.; Buback, C.; Curtin, B.; Acar, S.; Kolasinac, D.; Yin, W.; Rubenstein, D. A.; Lu, H.; Leventis, N.; Sotiriou-Leventis, C. Evaluation of Dysprosia Aerogels as Drug Delivery Systems: A Comparative Study with Random and Ordered Mesoporous Silicas. *ACS Appl. Mater. Interfaces* **2014**, *6*, 4891−4902.
(25) Su, B.-L, Clément, S., Yang, X.-Y. *Hierarchically Structured Porous Materials: From Nanoscience to Catalysis, Separation, Optics, Energy, and Life Science*; Wiley-VCH: Weinheim, Germany, 2011.
(26) Loiola, A. R.; da Silva, L. R. D.; Cubillas, P.; Anderson, M. W. Synthesis and Characterization of Hierarchical Porous Materials Incorporating a Cubic Mesoporous Phase. *J. Mater. Chem.* **2008**, *18*, 4985−4993.
(27) Tao, G.; Zhang, L.; Hua, Z.; Chen, Y.; Guo, L.; Zhang, J.; Shu, Z.; Gao, J.; Chen, H.; Wu, W.; Liu, Z.; Shi, J. Highly Efficient Adsorbents Based on Hierarchically Macro/Mesoporous Carbon Monoliths with Strong Hydrophobicity. *Carbon* **2014**, *66*, 547−559.
(28) Gao, L.; Sun, J.; Zhang, L.; Wang, J.; Ren, B. Influence of Different Structured Channels of Mesoporous Silicate on the Controlled Ibuprofen Delivery. *Mater. Chem. Phys.* **2012**, *135*, 786−797.
(29) Datt, A.; El-Maazawi, I.; Larsen, S. C. Aspirin Loading and Release from MCM-41 Functionalized with Aminopropyl Groups via Co-condensation or Postsynthesis Modification Methods. *J. Phys. Chem. C* **2012**, *116*, 18358−18366.
(30) Yoldas, B. E. Alumina Gels that form Porous Transparent Al_2O_3. *J. Mater. Sci.* **1975**, *10*, 1856−1860.
(31) Chen, M.; Zhang, C.; Li, X.; Zhang, L.; Ma, Y.; Zhang, L.; Xu, X.; Xia, F.; Wang, W.; Gao, J. A One-Step Method for Reduction and Self-Assembling of Graphene Oxide into Reduced Graphene Oxide Aerogels. *J. Mater. Chem. A* **2013**, *1*, 2869−2877.
(32) Baumann, T. F.; Gash, A. E.; Chinn, S. C.; Sawvel, A. M.; Maxwell, R. S.; Satcher, J. H. Synthesis of High-Surface-Area Alumina Aerogels without the Use of Alkoxide Precursors. *Chem. Mater.* **2005**, *17*, 395−401.
(33) Keysar, S.; Shter, G. E.; deHazan, Y.; Cohen, Y.; Grader, G. S. Heat Treatment of Alumina Aerogels. *Chem. Mater.* **1997**, *9*, 2464−2467.
(34) Chen, Q.; Udomsangpetch, C.; Shen, S. C.; Liu, Y. C.; Chen, Z.; Zeng, X. T. The Effect of AlOOH Boehmite Nanorods on Mechanical Property of Hybrid Composite Coatings. *Thin Solid Films* **2009**, *517*, 4871−4874.
(35) Jeon, S. J.; Lee, J. J.; Kim, W.; Chang, T. S.; Koo, S. M. Hard Coating Films Based on Organosilane-Modified Boehmite Nanoparticles under UV/Thermal Dual Curing. *Thin Solid Films* **2008**, *516*, 3904−3909.
(36) Nampi, P. P.; Moothetty, P.; Berry, F. J.; Mortimer, M.; Warrier, K. G. Aluminosilicates with Varying Alumina−Silica Ratios: Synthesis Via a Hybrid Sol−Gel Route and Structural Characterization. *Dalton Trans.* **2010**, *39*, 5101−5107.
(37) Priya, G. K.; Padmaja, P.; Warrier, K. G. K.; Damodaran, A. D.; Aruldhas, G. Dehydroxylation and High Temperature Phase Formation in Sol−Gel Boehmite Characterized by Fourier Transform Infrared Spectroscopy. *J. Mater. Sci. Lett.* **1997**, *16*, 1584−1587.
(38) Sreenivasulu, P.; Viswanadham, N.; Saxena, S. K. Facile Synthesis of Mesoporous Aluminosilicate Nanoparticles for the Selective Production of *N*-Benzylidenaniline in a Solvent-Free Reaction of Aniline with Benzyl Alcohol. *J. Mater. Chem. A* **2014**, *2*, 7354−7359.
(39) Liu, E.; Locke, A. J.; Martens, W. N.; Frost, R. L.; Yang, X. Fabrication of Macro−Mesoporous Zirconia−Alumina Materials with a One-Dimensional Hierarchical Structure. *Cryst. Growth Des.* **2012**, *12*, 1402−1410.
(40) Arachchige, I. U.; Brock, S. L. Sol−Gel Assembly of CdSe Nanoparticles to form Porous Aerogel Networks. *J. Am. Chem. Soc.* **2006**, *128*, 7964−7971.
(41) Bhosale, S. V. Yoctowell Cavities on Magnetic Silica Nanoparticles for pH Stimuli-Responsive Controlled Release of Drug Molecules. *Chem.—Eur. J.* **2014**, *20*, 5253−5257.
(42) Liong, M.; Angelos, S.; Choi, E.; Patel, K.; Stoddart, J. F.; Zink, J. I. Mesostructured Multifunctional Nanoparticles for Imaging and Drug Delivery. *J. Mater. Chem.* **2009**, *19*, 6251−6257.
(43) Bhosale, S. V.; Bhosale, S. V. Yoctowells as a Simple Model System for the Encapsulation and Controlled Release of Bioactive Molecules. *Sci. Rep.* **2013**, DOI: 10.1038/srep01982.
(44) Angelos, S.; Khashab, N. M.; Yang, Y.-W.; Trabolsi, A.; Khatib, H. A.; Stoddart, J. F.; Zink, J. I. pH Clock-Operated Mechanized Nanoparticles. *J. Am. Chem. Soc.* **2009**, *131*, 12912−12914.